Electrochemical detection of uric acid and ascorbic acid using r-GO/NPs based sensors

Francesca Mazzara[*1], Bernardo Patella[*1], Giuseppe Aiello[1], Alan O'Riordan[2], Claudia Torino[3], Antonio Vilasi[3], Rosalinda Inguanta[†1]

[1]Laboratorio Chimica Fisica Applicata, Dipartimento di Ingegneria, Università degli Studi di Palermo, Viale delle Scienze, 90128 Palermo

[2]Nanotechnology group, Tyndall National Institute, University College Cork, Dyke Prade, Cork, Ireland

[3]Laboratorio di Bioinformatica, Istituto di Fisiologia Clinica (IFC)-Consiglio Nazionale delle Ricerche-Reggio Calabria-Italy

ABSTRACT

A sensitive and selective electrochemical sensor, based on reduced graphene oxide and gold nanoparticles obtained by simple co-electrodeposition, was developed for the detection of uric acid and ascorbic acid. Because of the electrochemical oxidation of both uric and ascorbic acid depending on the pH, the sensor performances were studied at different pH values. Excellent results were obtained for uric acid detection in a linear range from 10 to 500 µmol dm^{-3} with a sensitivity of 0.31 µA cm^{-2} μM^{-1}. A limit of detection and quantification of 3.6 µM and 10.95 µmol dm^{-3}, respectively, was calculated. Sensors showed good selectivity toward different interfering species present in the matrix of milk, fruit juice and urine (Na^+, NH_4^+, Cl^- and glucose). A simultaneous detection of uric acid and ascorbic acid was also carried out reaching a limit of detection of 2.26 and 5.63 µmol dm^{-3}, respectively. Sensors were also validated measuring both acids in real samples of foods and body fluids (commercial milk and fruit juice and urine). Excellent results were achieved in good agreement with conventional techniques.

[*] These authors contributed equally to this work.
[†] Corresponding Author: Rosalinda Inguanta, rosalinda.inguanta@unipa.it

KEYWORDS: Electrochemical Sensor, Ascorbic Acid, Uric acid, Food, Body fluids.

1. INTRODUCTION

Uric acid (UA) and ascorbic acid (AA) are two common antioxidant that frequently coexist in food and biological samples [1]. Different values, even in the concentration range normally present in human body and foods, can cause several health problems and food quality alteration.

UA is a natural waste product of the metabolic breakdown of purines [2,3]. In blood and urine, normal levels of UA range from 0.14 to 0.4 mmol dm^{-3} [4] and from 1.5 to 4.5 mmol dm^{-3} [5], respectively. Many factors can alter these values such as age and gender [6]. High level of UA in blood plasma causes hyperuricemia, which in turn may lead to gout disease [7] and increase the risk of cardiovascular diseases [8], Lesch–Nyhan syndrome [9] and type 2 diabete [10]. On the other hand, low levels of UA can be related to multiple sclerosis, Parkinson and Alzheimer diseases [11].

AA (vitamin C), due to its antioxidant properties, is usually added to many foods and beverage to improve the appearance of preserved items [12]. It is also used as a colour and flavour stabilizer and browning inhibitor [13]. In the human body, AA is essential for carnitine, collagen and neurotransmitters biosynthesis [14]. European Food Safety Authority has established that the average supply of AA, coming by food intake, is about 90 mg/day in healthy adults [15]. Higher levels of AA can lead to undesired gastrointestinal and renal effects, related to inflammatory reactions and excretion of oxalate with urine, respectively [16]. Instead, a low assumption of AA causes scurvy, a pathology related to collagen synthesis [17]. Moreover, AA deficiency affects the immune system, iron absorption and cholesterol and protein metabolism [18].

For all these reasons, it is important to evaluate UA and AA concentration in both food and human body fluids. To measure UA and AA, various methods have been employed, such as titration [19], capillary electrophoresis [20], liquid chromatography [21] and spectrophotometric [22]. These

methods present many drawbacks, such as the overestimation of the acid concentration [23]. Furthermore, they are laboratory-based techniques that require highly skilled personnel, expensive equipment and reagents and cannot be performed in situ and/or in real time [24–26].

Considering that UA and AA can be easily electrochemically oxidized in aqueous solutions, their electrochemical detection (by cyclic voltammetry, differential pulse voltammetry and amperometry) is a valid, fast and simple, as well as sensitive and selective, method [27]. Many different sensors for UA and AA detection have been developed, and different sensing materials have been employed in order to maximize the selectivity [1,27–29]. Graphene is a suitable material for electrochemical detection because of its excellent properties [30–32], such as high surface to volume ratio, abundant defects and fast electron transfer rates [33]. Also graphene-composite electrodes ensures large specific surface area and high electrical conductivity [34] leading sensors with excellent performances. Nithya et al. [35] developed an electrochemical sensor based on ZnO-decorated with reduced graphene oxide (rGO) on glassy carbon electrode (ZnO-rGO-GCE) to detect AA in pharmaceutical formulations and fruit extracts. Due to the high electroactive surface area, 3.5 times higher compared to the bare electrode, ZnO-rGO-GCE sensor allows to achieve a sensitivity of 0.178 $\mu A\ \mu M^{-1} cm^{-2}$ and a limit of detection (LOD) 0.01 $\mu mol\ dm^{-3}$. This is also the approach followed by Tukimin et al [36], who proposed a composite electrode of rGO and PEDOT (poly(3,4-ethylenedioxythiophene) showing very good performance for UA detection in a wide linear range.

To further improve the electrochemical performance of graphene, the coupling with nanoparticles (NPs) was also proposed, because, due to unique catalytic and electronic properties, NPs accelerate electron transfer and reduce overvoltage of electrochemical process [37–39]. NPs are very useful for the simultaneous detection of UA and AA, because one of the main drawbacks is related to their very similar oxidation peak potentials, making very complicate their electrochemical

identification. This is particularly true in biological fluids due to the presence of dopamine (DA) [1] whose oxidation peak is very close to UA e AA. The use of electrodes modified with noble metals NPs was the winning strategy to overcome this problem [40]. For example electrodes decorated with Pt NPs [41] and Au NPs [42] permitted to obtain well-resolved oxidation peaks with also very good results in terms of sensitivity and LOD.

In our previous work [43], we reported preliminary results on the development of an electrochemical sensor based on gold NPs and r-GO for AA detection. In particular, we showed that the functionalization of indium tin oxide (ITO) based electrodes with both rGO and AuNPs is a valid approach to obtain good sensor features. In fact, the presence of both rGO and AuNPs ensures high current density at low potential values, leading to a selective and sensitive sensor. Here, we perform a systematic investigation on this type of sensors for UA e AA detection studying also their simultaneous analysis. The sensors were carefully characterized from both the chemical-physical (by XRD, SEM and EDS) and electrochemical point of view, through the evaluation of the electrochemical active surface area (ECSA). Moreover, the sensors were validated detecting UA and AA in real samples (milk, fruit juice and urine), also verifying the possible interference coming from the different species present in their matrix.

2. EXPERIMENTAL

ITO/PET sheets, iso-propanol, $KAuCl_4$, Sodium Acetate, Acetic Acid, aqueous Graphene Oxide suspension (4 mg/ml), Potassium hydrogen phosphate, Potassium dihydrogen phosphate, AA, UA, Potassium hydroxide, Sulfuric acid were purchased from Sigma Aldrich. All chemicals were used as received and dissolved in ultrapure water (Type 1, with a resistivity greater than 18 MΩ·cm).

The ITO-PET sheets were polished with an ultrasonic cleaner using pure iso-propanol and distillated water and dried in air for further use. Electrochemical fabrication and characterization were carried out using a homemade cell, fabricated using a Zortrax 3D printer, with a volume of 1 mL. The sensors were obtained by simple co-electrodeposition following the optimized procedure detailed in our previous works [38,44,45]. In particular, an acetate buffer solution (ABS) at pH 5, containing of 0.25 mmol dm^{-3} $KAuCl_4$ and 0.5 mg/ml GO was used as deposition bath. The co-electrodeposition was carried out at -0.8 V vs SCE for 200 s in air and at room temperature [38,46]. Electrodes were characterized by X-ray diffraction (XRD) using a RIGAKU diffractometer (model: D-MAX 25600 HK). All diffractograms were obtained in the 2θ range from 5° to 100° with a step of 0.02° and a measuring time of 0.5 sec for step, using the copper Kα radiation (λ= 1.54 Å), using a tube voltage of 40 kV and a current of 30 mA. Diffraction patterns were analysed by comparison with literature data. Morphology was analysed by scanning electron microscopic (SEM) using a FEI FEG-ESEM (model QUANTA 200) provided with X-ray Energy Dispersive probe (EDS). SEM/EDS analyses were performed using an acceleration voltage of 30KV at a working distance of 10 mm. EDS spectra were collected using the frame-mode (exanimated area 3.2x3.2 μm) and, to acquire a statistically significant number of counts, the analysis was performed for at least 300 sec. Different areas of the samples were analysed to verify the uniformity of deposition. Major details on characterization methods can be found in [47,48]. Electrochemical deposition and characterization were performed with a PARSTAT 2273 electrochemical workstation using a Pt wire as a counter electrode and a saturated calomel electrode (SCE) as reference electrode. For characterization, phosphate buffer (PBS, pH 8) solution was used. The effect of scan rate on AA and UA detection was studied in the range from 5-1000 mV s^{-1} using a solution of 0.2 mmol dm^{-3} of AA or UA. In order to calculate the double layer capacitance, CVs at different scan rate

(20-100 mV s^{-1}) were carried out in PBS solution in a potential range without faradic processes. All electrochemical analyses were carried out in a not mechanically agitated solution, which was replaced at the end of each test, and at room temperature. Some tests, in particular for milk analysis, were performed in nitrate solution (0.1 M) to avoid the precipitation of calcium compounds which made analysis impossible. Cyclic voltammetry (CV) study was performed at different scan rates, and some tests were carried out in de-aerated solution by N_2 purging.

Sensor performances were evaluated by Linear Sweep Voltammetry (LSV) at different pH (from 6 to 9). The calibration curve was obtained using the subtract baseline method, and thus those corresponding to maximum were selected as peak potential and current density. Interference tests were performed toward different species typically present in body fluids and food (dopamine, Na^+, NH_4^+, Cl^- and glucose) matrix. Sensors were also validated in real samples (milk, fruit juice and urine) to compare our results with those obtained with conventional techniques.

All tests reported in this work were repeated three times using a new electrode and fresh solution for each test and the main value was plotted to calculate the main properties of the sensor. The obtained data were statically compared using GraphPad Prism 6.0 software, identifying the differences by one-way repeated measures analysis of variance with Bonferroni post hoc test. A P value < 0.05 was considered significant.

3. RESULTS AND DISCUSSION

3.1. Fabrication and characterization of Au NPs/rGO- modified electrode

The optimized deposition process led to the co-deposition of AuNPs and rGO with a balanced loading that ensures a high electrochemical surface area, resulting in a good electrocatalytic activity for oxidation of AA and UA. The typical morphology can be observed in the SEM

images of Figure 1. In particular, in Figure 1a it is clear the presence of rGO micro-sheets while Figure 1b shows the AuNPs having a medium diameter of about 30±5 nm.

The co-electrodeposition of rGO and Au-NPs occurred following the reactions [49,50]

$$GO + xH^+ + ye^- \rightarrow rGO + zH_2O \quad (1)$$

$$AuCl_4^- + 3e^- \rightarrow Au + 4Cl^- \quad (2)$$

These reactions led to deposition of rGO micro-sheets that were simultaneously almost uniformly covered with Au nanoparticles. In the entire area (about 0.8 cm^2) of electrode both rGO and Au NPs are clearly present, and this was also confirmed by XRD and EDS analyses. In the EDS spectrum, Figure 1c, it is possible to observe Au peak from NPs, carbon and oxygen peaks coming mainly from the PET substrate and the electrodeposited rGO. The indium peaks, overlapping tin peaks, come from the ITO coating. EDS was performed in different area of the electrode to confirm the uniformity of deposition. XRD diffraction, Figure 1d, also reveals the presence of rGO and AuNPs. In particular, the broad peak at 2θ of about 24.5 is assigned to (002) characteristic plane of reduced graphene oxide [51]. The diffraction peaks at about 38.2°, 44.4°, 64.6° and 77.5°, correspond to (111), (200), (220), (311) plans of Au NPs, respectively [52]. The mean grain size of Au NPs was evaluated by Sherrer's equation [53]:

$$d_g = \frac{K\lambda}{\beta cos\theta}$$

Where d_g is the grain size, K is the shape factor fixed at 0.9, λ is the X-ray wavelength, β is the width at half height of the main peak and θ is the Bragg angle. Results shows a mean value of about 31±0.17 nm consistent with SEM measurements. The others diffraction peaks correspond to ITO phase.

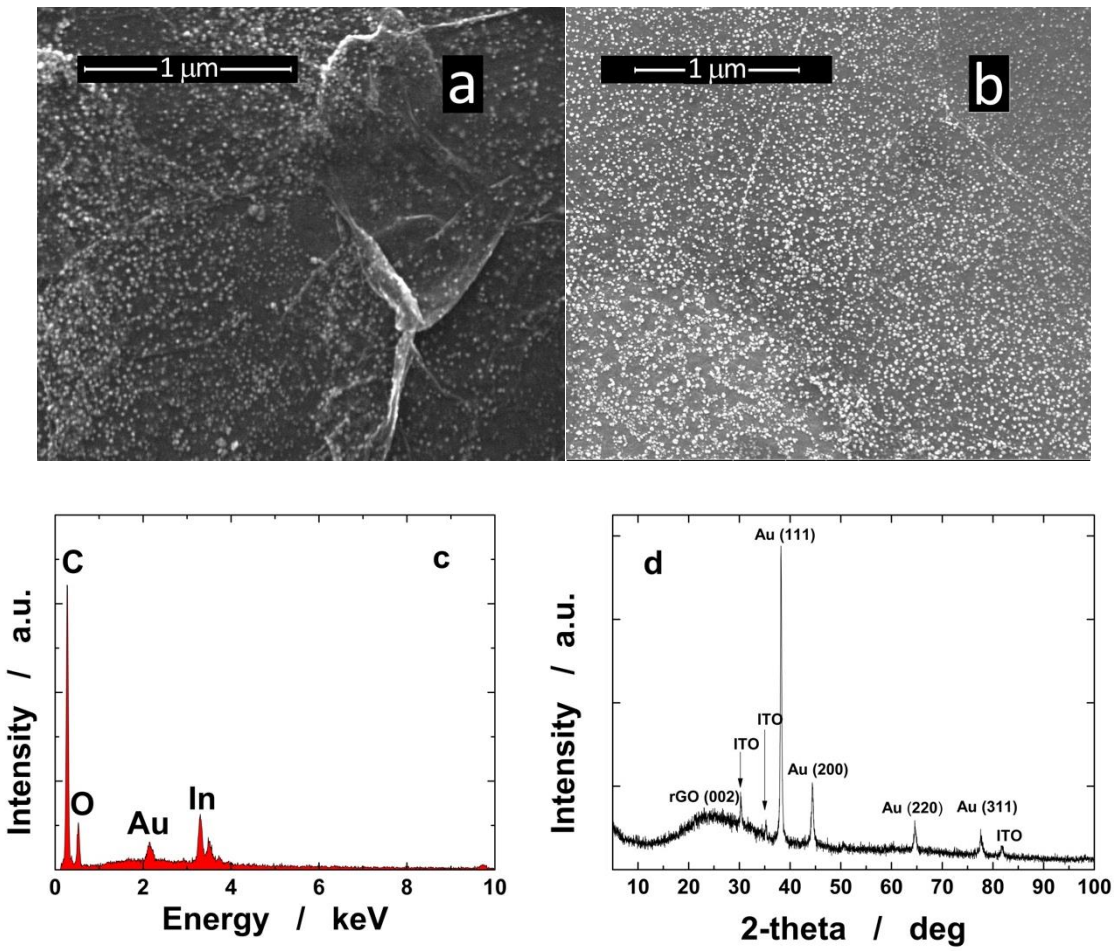

Figure 1. (a, b) Typical SEM images, (c) EDS spectrum, and (d) XRD pattern of ITO-rGO-AuNPs electrode

To study how the substrate modification improves the electrochemical performances of the sensors, the double layer capacitance (C_{dL}) was evaluated by carrying out cyclovoltammetry tests (CVs) at different scan rates using a blank solution (without AA or UA added) of PBS at pH 7, in a potential range without faradic processes [54,55]. To better compare the results, this test was carried out using bare ITO, ITO-AuNPs, ITO-rGO and ITO-rGO-AuNPs electrodes. The plot of the difference of double layer charging current density $\Delta i=(i_a-i_c)$ increases linearly with scan rate and its slope is related to C_{dL}.

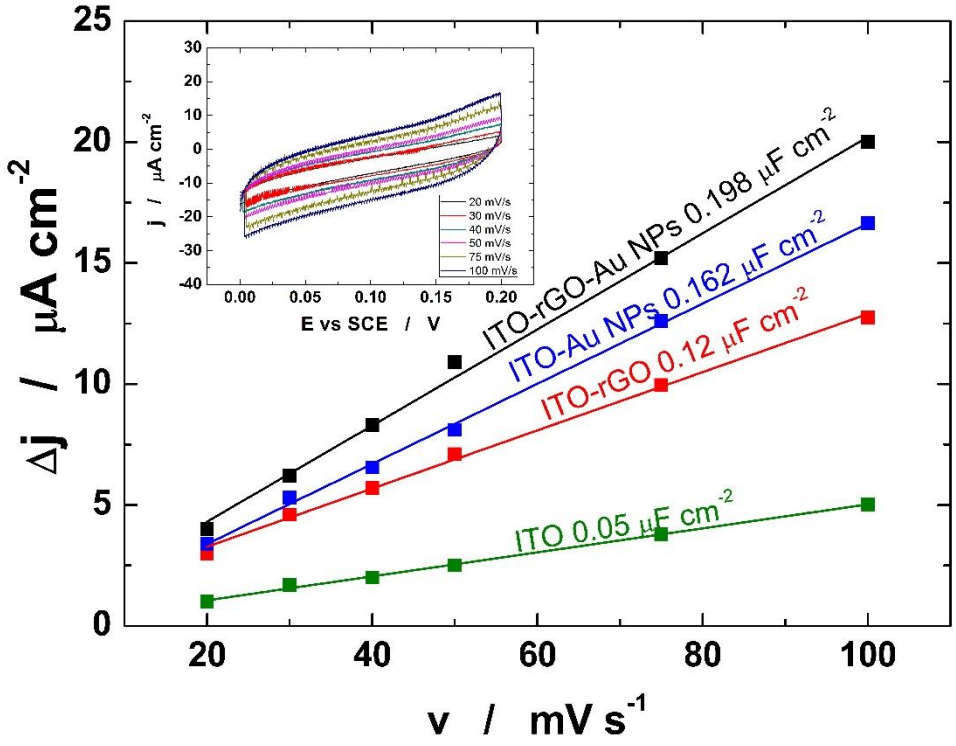

Figure 2. Double layer charging current density plotted as a function of scan rate. Tests were performed in a potential range from 0.00 V to 0.2 V vs SCE in PBS (pH 8) and at room temperature.

Figure 2 shows that C_{dL} of bare ITO is very small (0.05 μF cm^{-2}). The modification of ITO with the deposition of rGO and Au NPs causes an increase of C_{dL} of about 140% and 225%, respectively. Obviously, due to a nanostructured morphology, the presence of NPs leads to a greater increase in C_{dL} than the rGO micro-sheets. Interestingly, in the case of ITO modified with both Au NPs and rGO, the higher C_{dL} value was found (0.198 μF cm^{-2}, the inset of Figure 2 shows the CVs carried out using the ITO-rGO-AuNPs electrode) with an increase of about 295% with respect to bare ITO. Considering that the C_{dL} is related to the real electrochemical active surface area (ESCA), these results demonstrate that the co-deposition of Au NPs and rGO is an excellent method to modify the electrode because it ensures a high active surface area and thus high electroactivity [54].

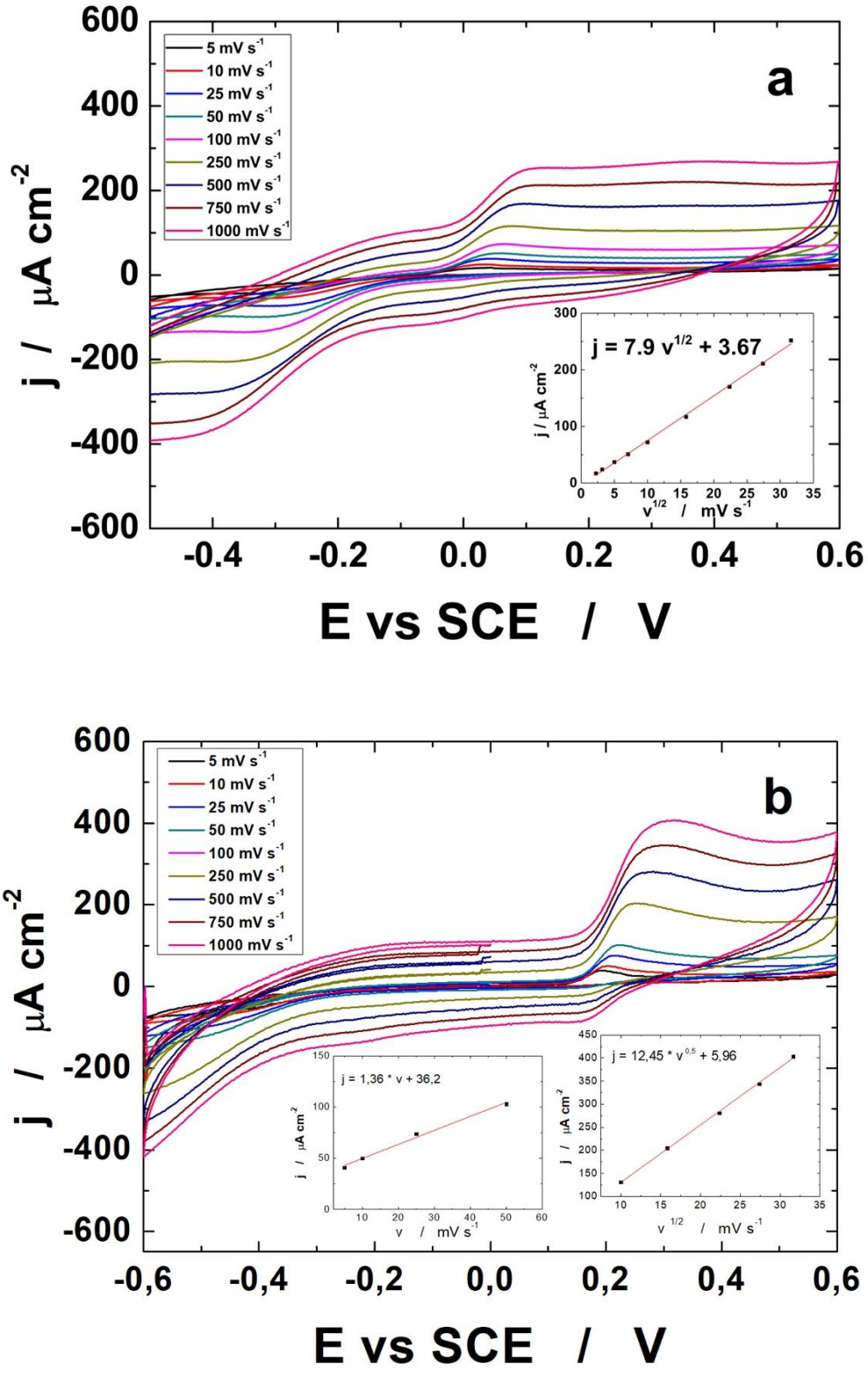

Figure 3 Effect of scan rates on CV response of 200 µM of (a) AA in PBS pH 7 and (b) UA in PBS pH 8. CVs were performed in a potential range from -0.6 V to 0.6 V vs. SCE at room temperature.

The electrochemical oxidation of AA and UA using ITO-rGO-AuNPs electrode was studied by CVs performed at different scan rates (v), from 5 to 100 mV/s, using PBS with 0.2 mmol dm^{-3} of AA and 0.2 mmol dm^{-3} UA, Figure 3. For AA, Figure 3a shows the linear increase of peak current density with the square root of scan rate, suggesting a diffusion-controlled process [56]. This result agrees with data obtained by Březina et al [57].

In the case of electrochemical oxidation of UA, Figure 3b, as reported in [36,58], at low scan rate the oxidation is adsorption-controlled process and in fact a direct proportionality was found between the peak current density and the scan rate. At high scan rate, the UA oxidation becomes a diffusion-controlled process.

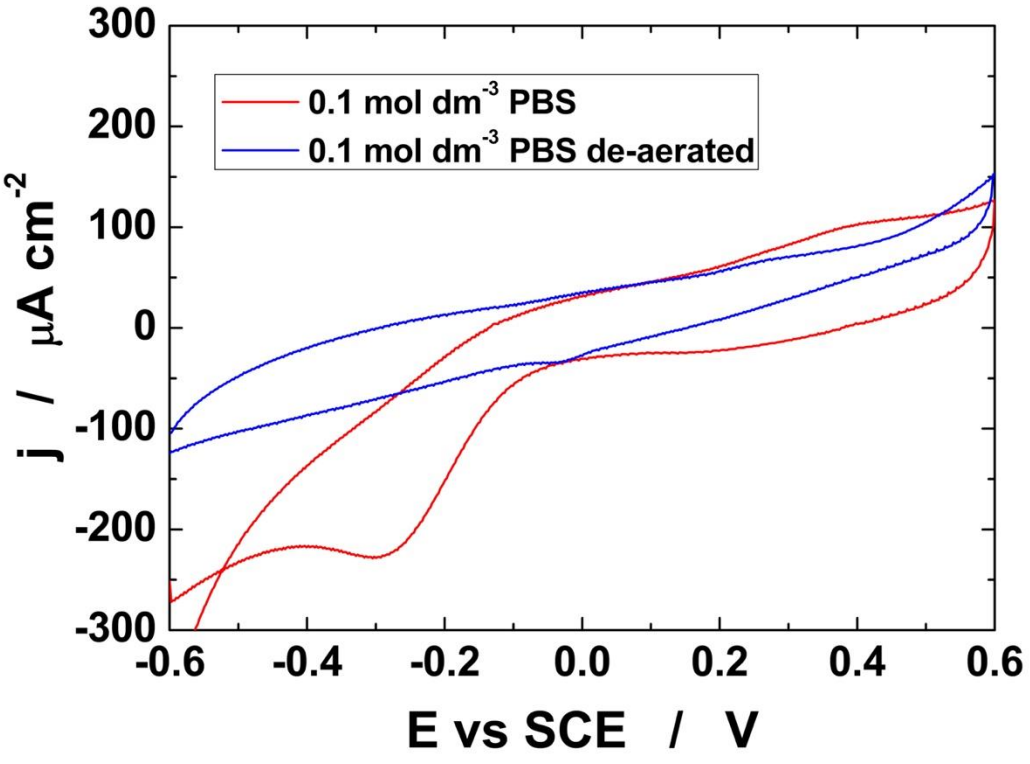

Figure 4 LSV response of blank solution in aerated and de-aerated conditions. LSV curves were recorded in the potential range from +0.6 V to -1 V vs SCE with a scan rate of 20 mV s^{-1}, in PBS (pH 8) at room temperature.

The AA oxidation process can be considered irreversible because of the absence of reduction peak [36,57,58]. The peak at about -0.3 V vs SCE, clearly present in Figure 3a, is related to the reduction of dissolved oxygen to hydrogen peroxide [59]. This statement has been proved by the CVs of the blank solution of PBS carried out in aerated and de-aerated conditions, reported in Figure 4. It can be observed that the peak located at -0.4 V is present only in aerated condition, hence its attribution to hydrogen peroxide generation from reduction of dissolved oxygen.

The slope of logj vs. log*v*, Figure 5, corresponds to the heterogeneous charge transfer coefficient (α) [60,61]. For AA and UA, the calculated values are about 0.501 and 0.451, respectively. For the AA the value is equal to theoretical one (0.5), this is a further confirm that AA oxidation is a diffusion-controlled processes.

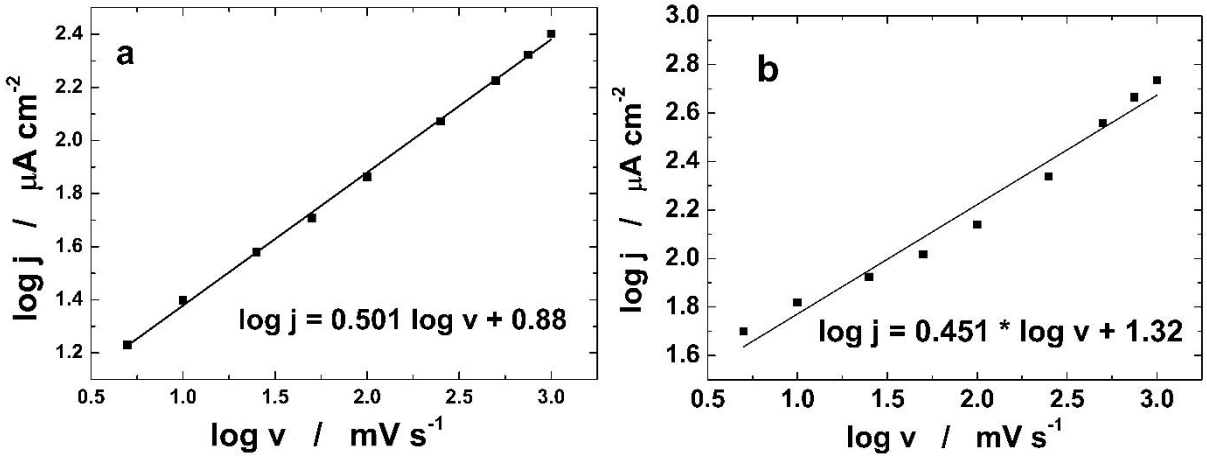

Figure 5 Oxidation current density (μA/cm^{-2}) of AA (a) and UA (b) vs. scan rate (mV s^{-1}): (a) AA in PBS pH 7 and (b) UA in PBS pH 8. CVs were performed in a potential range from -0.6 V to 0.6 V vs. SCE at room temperature.

The values of α were used to calculate the number of electrons (n) involved in the AA and UA oxidation by the following equation [60,61]:

$$Ep - Ep_{0.5} = \frac{47.7}{\alpha\, n}$$

where E_p is the peak potential and $E_{p0.5}$ is the half peak potential. Using this equation, the number of electrons for AA and UA oxidation was estimated to be equals to 2 (esteemed values 2.14 and 1.98, respectively) according to the mechanism proposed by Kannan et al [62].

3.2. Effect of pH on electrochemical detection of UA and AA

The oxidation reactions of UA and AA highly depends on the pH thus this parameter plays a crucial role on their electrochemical detection [63]. To verify this, the pH of blank solution was changed from 6 to 9 both for UA and AA. In Figure 6 the peak current intensity and the peak potential vs pH was reported.

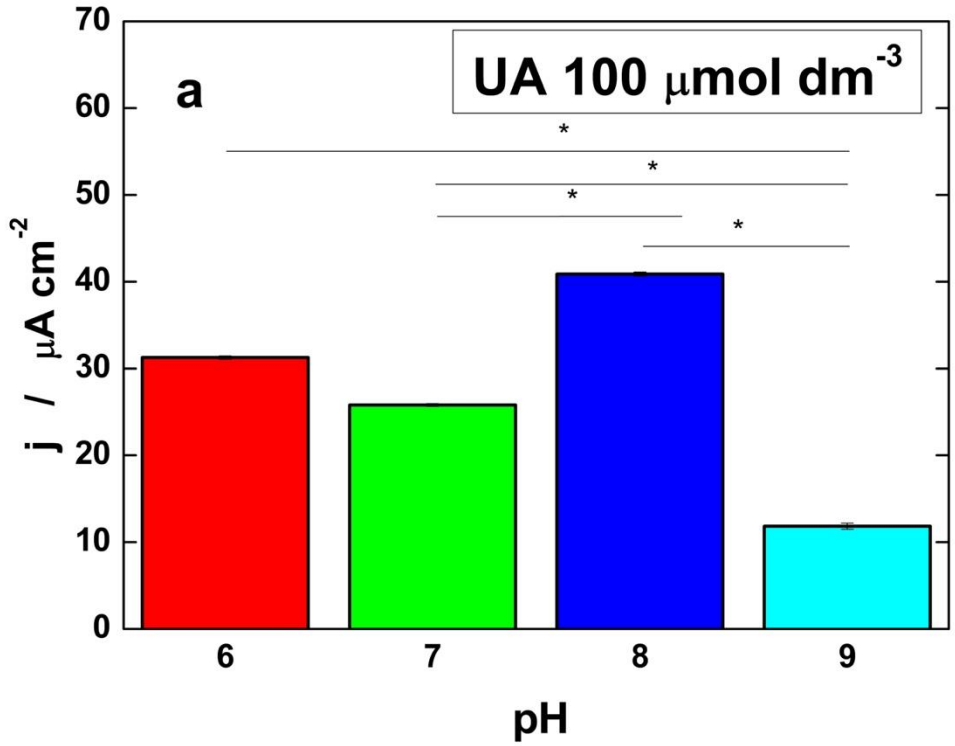

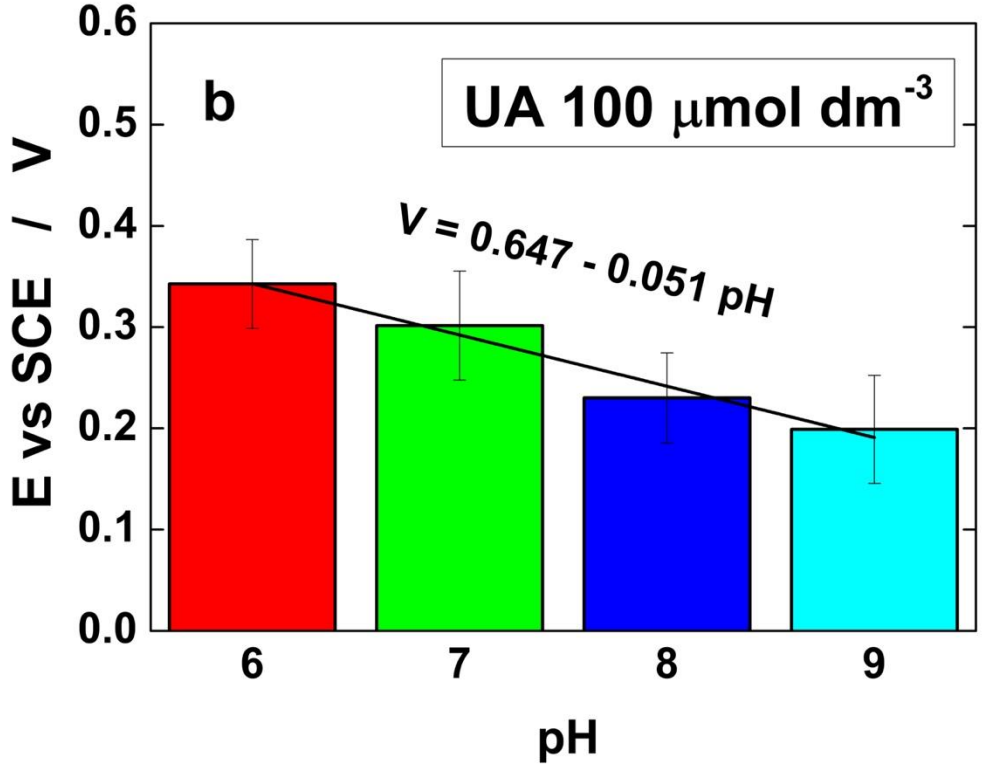
b
UA 100 μmol dm-3
V = 0.647 - 0.051 pH
E vs SCE / V
0.6
0.5
0.4
0.3
0.2
0.1
0.0
6
7
8
9
pH

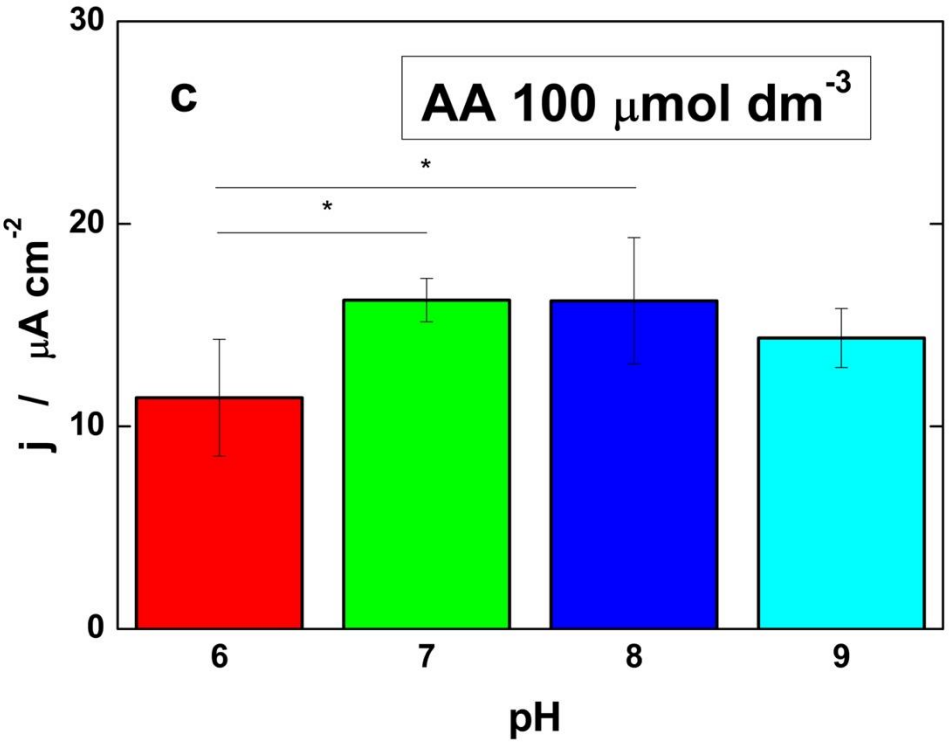
c
AA 100 μmol dm-3
*
*
j / μA cm-2
30
20
10
0
6
7
8
9
pH

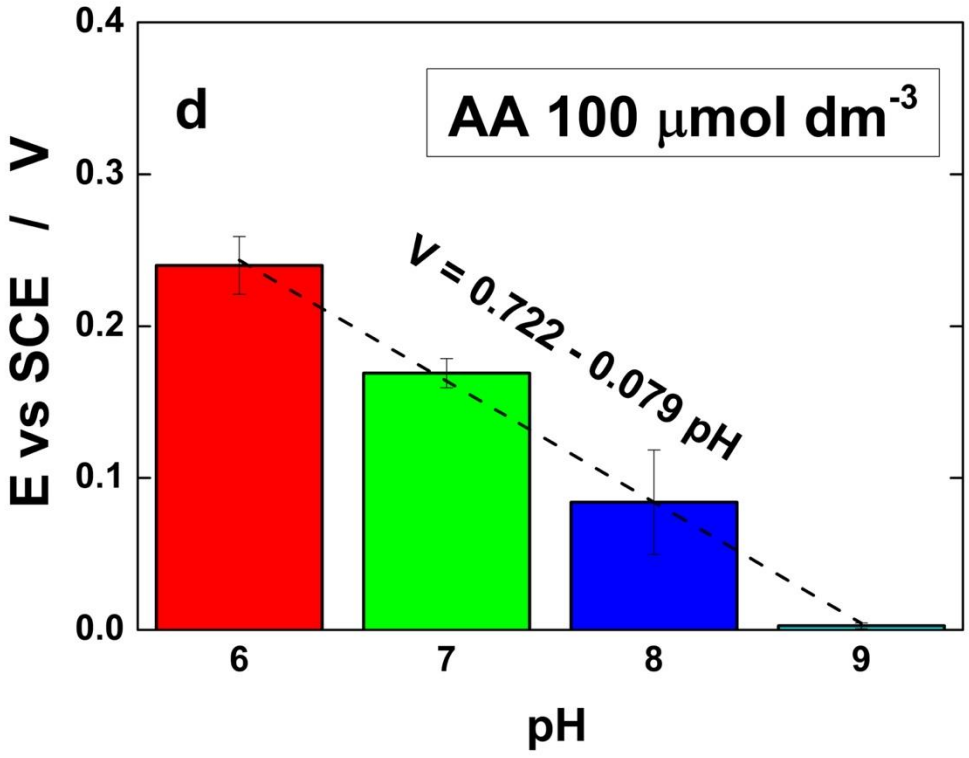

Figure 6 Effect of solution pH on the current density and peak potential for the detection of (a-b) 100 µmol dm^{-3} UA and (c-d) 100 µmol dm^{-3} of AA.

As showed in Figure 6a, the peak current is more intense at pH 8 than at the other values. Figure 6b shows that the peak potential shift toward more cathodic values with increasing the solution pH. A linear dependence was found with a slope of about -51 mV/pH unit. This value suggests that the electrochemical oxidation of UA followed the Nernst equation according to [1], involving two protons and two electrons. For AA, the best results in terms of peak current (Figure 6c) was obtained at pH 7 and 8 even if at pH 7 a most acceptable values of standard deviation for both current intensity and peak potential (Figure 6d) was obtained. Also for AA a linear dependence was found with a slope of about -79 mV/pH unit. Considering these results, pH 8 was chosen as the best value for the following electrochemical detection of both UA and AA.

3.3. Sensor performance

In order to perform quantitative AA and UA analysis, LSV was employed as electrochemical technique using ITO-rGO-AuNPs as working electrode. For AA, Figure 7a shows that its detection starts at a concentration of 20 µmol dm^{-3} and linearly increases up to 150 µmol dm^{-3} of AA with a sensitivity of 0.118 µA μM^{-1}. For UA, Figure 7b, the detection starts for 10 µmol dm^{-3} and the linear range extends up to 500 µmol dm^{-3} with a sensitivity of 0.31 µA μM^{-1}. From these results, it can be concluded that ITO-rGO-AuNPs based electrodes have better performance toward UA compared to AA.

The limit of detection (LOD) and the limit of quantification (LOQ) were calculated using the following equations:

$$LOD = 3.3\ \frac{SD}{S}$$

$$LOQ = 10\ \frac{SD}{S}$$

where SD is the Standard Deviation of the blank signal and S is the sensitivity of the sensor. The calculated values for LOD are 3.1 and 3.6 µmol dm^{-3} for AA and UA respectively. For LOQ the values are 9.4 and 10.95 µmol dm^{-3} for AA and UA respectively. As it can be seen from Figure 7, the mean RSD of each experiment is about 2.2% for AA and 5.4% for UA. Considering that this value was obtained using a new and fresh electrode for each concentration, it contains both reproducibility and repeatability errors. The RSD values suggest that the fabrication method here used to obtain the sensor is reproducible and repeatable and thus permits to obtain sensors with same properties.

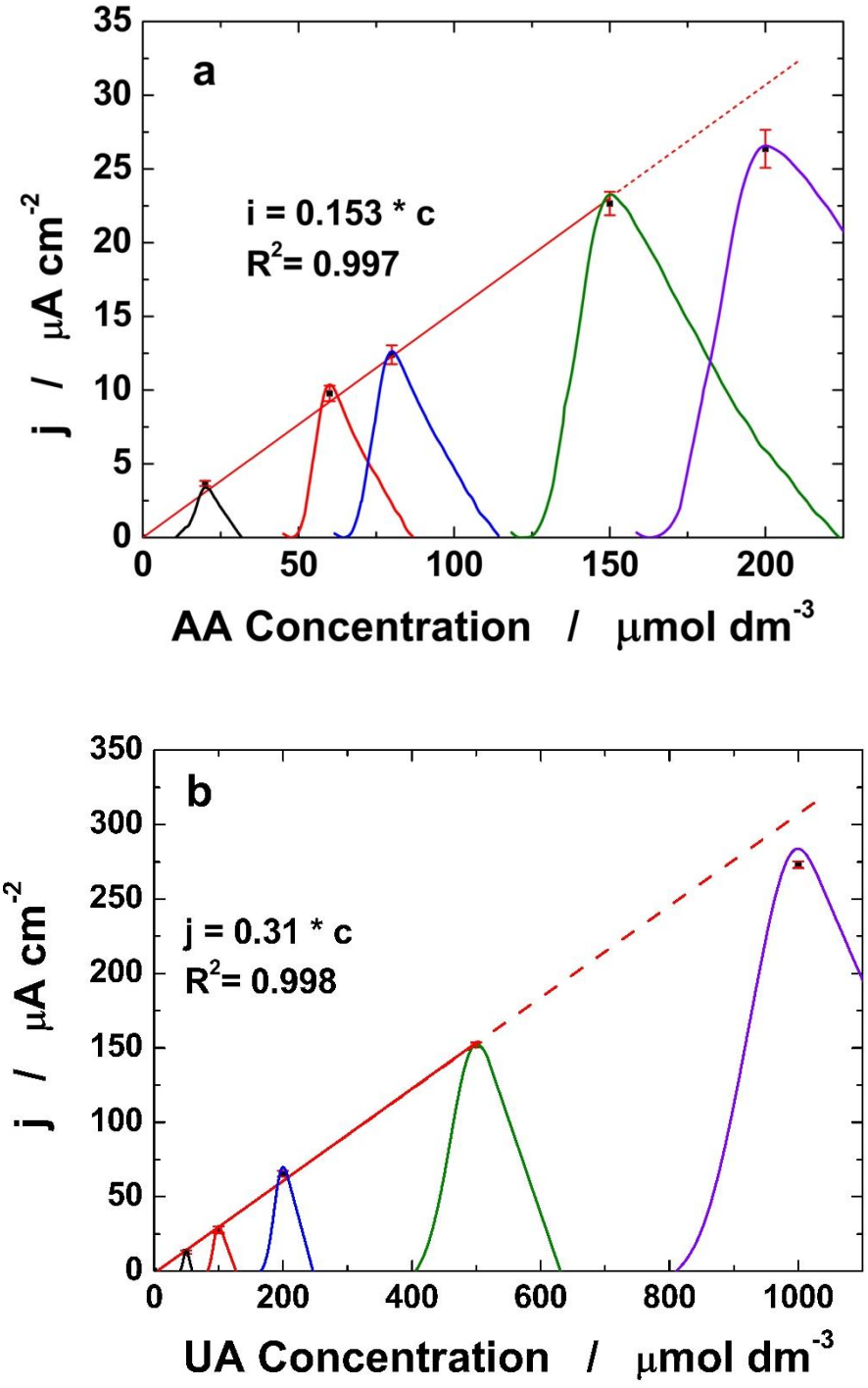

Figure 7 (a) Calibration of AA and (b) UA in PBS at pH 8

In order to verify the selectivity of ITO-rGO-AuNPs electrodes, the influence of various interfering species present in the matrix of real samples of foods and body fluids was studied. In particular,

the main constituents of milk, fruit juice and urine (sodium, chloride, glucose, dopamine and ammonia [64] [65]) were tested.

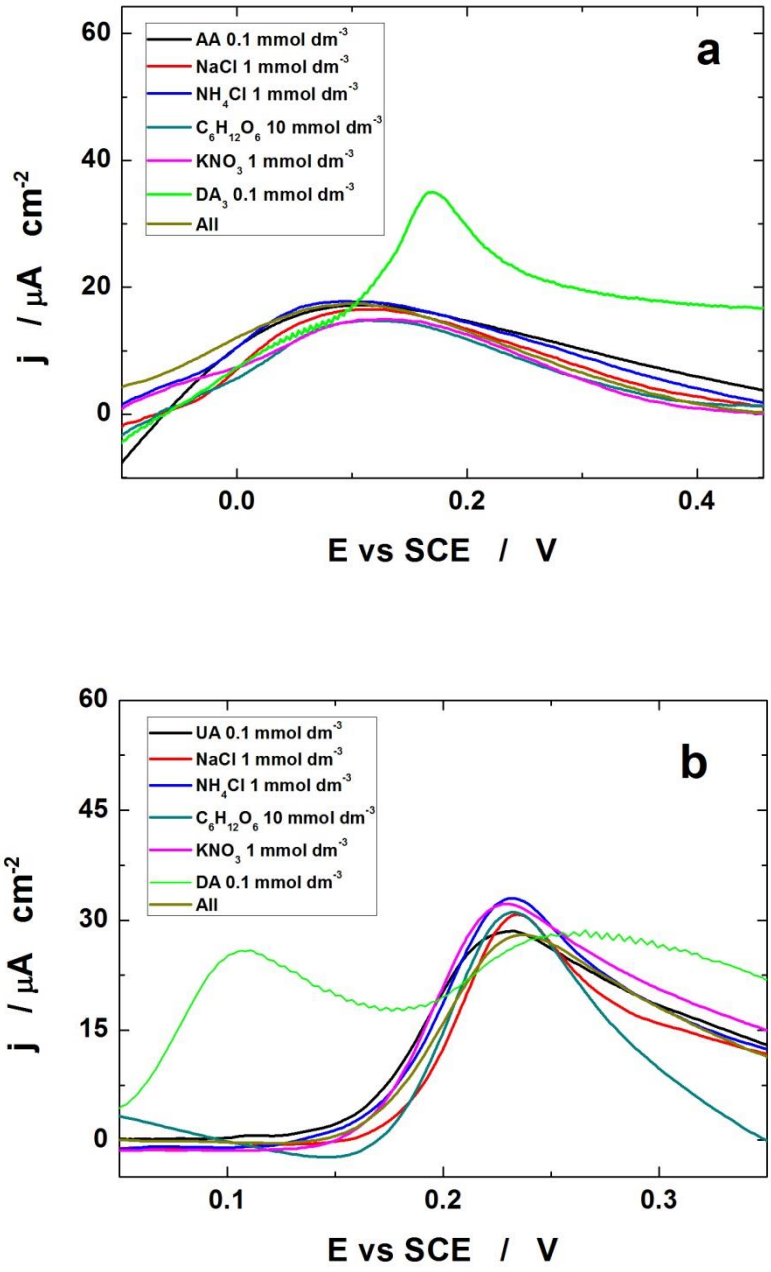

Figure 8 LSV curves showing the effect of interfering species on 0.1 mmol dm^{-3} of (a) AA and (b) UA detection. LSV tests were performed in a potential range from -0.5 V to 0.8 V vs. SCE with a scan rate 20 mV s^{-1} in PBS (at pH 7 for AA and at pH8 for UA) at room temperature.

Due to the bad solubility of calcium compounds in PBS, the interference tests for milk constituents were carried out also in $NaNO_3$ solution. In detail, 1 mM of Na^+, NH_4^+, K^+, NO_3^-, 2 mM of Cl^-, 10 mM of glucose, 0.1 mM DA were injected into a phosphate buffer solution also containing 0.1 mM of AA and 0.1 mM of UA, respectively. The results are showed in Figures 8a and 8b. Although the concentration of the interferents is 10 times higher than the concentration of AA and UA, there are negligible interference effects in their determination. The interference of dopamine (DA), one of the major possible interferers in the case of body fluids, was studied in details. In particular, Figures 8 shows the peak current density of AA (8a) and UA (8b) oxidation in presence of 0.1 mM of DA. The voltammogram shape changes dramatically in presence of high DA content, as shown in Figures 8. Indeed, a new peak appears, related to DA oxidation, at potential of about 0.11 V and 0.17 V vs SCE for UA and AA respectively. This difference in peak potential is due to the different pH for AA and UA detection [66]. In case of UA oxidation in the presence of DA the peak current density is almost unchanged. For AA, the oxidation peaks of AA and DA start to overlap, even if the AA peak is still noticeable. By the way, DA concentration in human body fluids ranges from 0.0001 mM to 0.001 mM [67] and thus the scenario of Figures 8 is practically unrealistic and very conservative. Figure S1 show the effect of lower DA concentration on AA and UA detection and an almost negligible effect was found. Thus, from these results it can therefore be concluded that the sensor proposed in this work has a high selectivity towards the main constituents of the matrix of the real samples.

Simultaneous detection of UA and AA with the ITO-rGO-AuNPs electrodes was also carried out. As shown in Figure 9, two separated peaks were obtained, located at 0.05 and 0.26 V vs. SCE, corresponding respectively to the oxidation of AA and UA. For both peaks, the current density increases in parallel with the concentration of analytes. A linear range from 20 to 100 µmol dm^{-3} was observed both for UA and AA with a LOD of 2.26 and 5.63 µmol dm^{-3} respectively. Thus,

using ITO-rGO-AuNPs electrodes the simultaneous detection of AA and UA is possible even if in a linear range lower than that found for both single analytes but without a loss in sensitivity that practically remained unvaried.

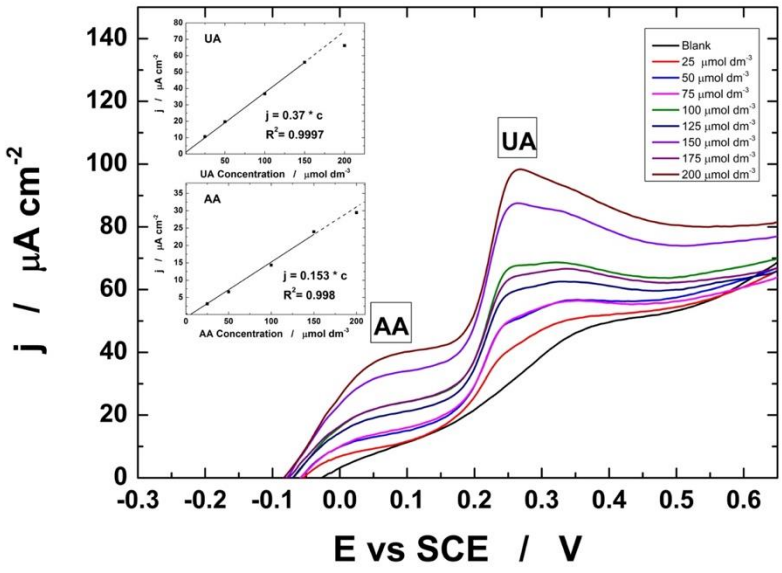

Figure 9 Simultaneous detection of UA and AA in PBS at pH 8. The LSV curves were recorded in the potential range from -0.5 V to 0.8 V vs SCE with a scan rate of 20 mV s^{-1} in PBS pH 8 at room temperature.

The stability of the sensors was also evaluated and the results were reported in Figure 10. In particular, as proposed in literature [68–70], sensor stability was evaluated as the % of current density variation after consecutive CV scans. Considering that for both acids the oxidation is an irreversible reaction, AA and UA solutions were replaced between each cycle. The results show that the UA current density decreases of 4.8%, 8.1% and 11% after 20, 30 and 75 consecutive scans, respectively. For AA, the current density decreases of 3.5% only after 75 cycles. Increasing the CV scans up to 100, the current density for both AA and UA oxidation decreases significantly (blue curves). Besides, in the case of AA oxidation, the peak potential shifts of about 0.03 V after 20 cycles. From these results, it can be concluded that the proposed sensor is stable for about 75 cycles.

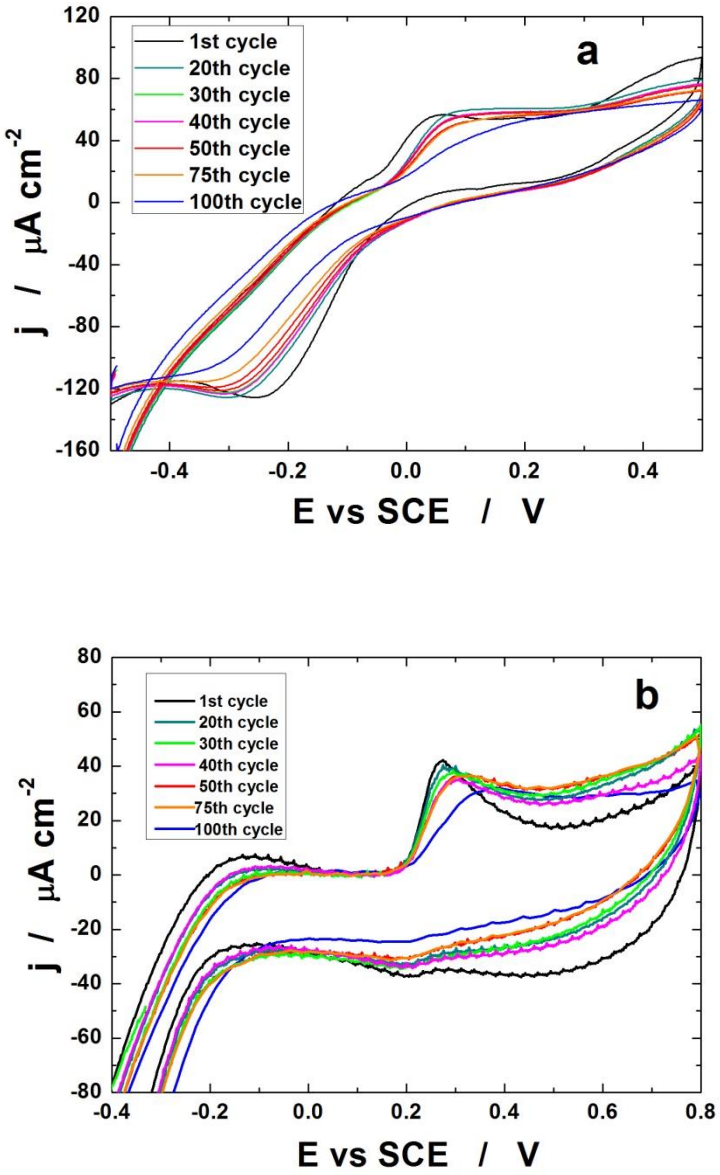

Figure 10 Stability of the sensors evaluated for 100 consecutive CV scans: a) AA and b) UA. CV tests were performed in a potential range from -0.5 V to 0.8 V vs. SCE for UA oxidation and from -0.5 V to 0.5V vs SCE for AA oxidation with a scan rate 100 mV s^{-1} in PBS (at pH 7 for AA and at pH8 for UA) at room temperature

3.4. Real samples analysis

To validate the sensor in real samples, the ITO-rGO-AuNPs electrodes were used to detect AA e UA in commercial milk and fruit juice and urine. A typical composition of these sample can be found in [67,71,72].

In all cases the standard addition method [73] has been applied to find the analytes concentration. Milk, juice and urine were split into several aliquots of the same volume. A known and increasing volume of standard solution of analyte was added to each one of these. Each solution was analysed by LSV technique, and the peak current density was plotted versus volume of standard solution of analyte. The slope and y-intercept of the linear regression were used to calculate the initial concentration of analyte in each sample. The obtained results are summarized in Table 1. Obtained results are in good agreement with those obtained by standard techniques and thus it is possible conclude that ITO-rGO-AuNPs electrodes have suitable behavior for real sample analysis.

Table 1 Result of UA and AA investigation on real samples employng ITO-rGO-AuNPs electrode

Sample	**Analyte**	**Supporting Electrolyte**	**Assayed [µmol dm^{-3}]**	**Final [µmol dm^{-3}]**	**Ref [µmol dm^{-3}]**
Milk	UA	$NaNO_3$	7.2	103 (± 17)	100-200 [74,75]
Juice	AA	PBS	76	1520 (± 200)	1820 Fig. S2
Urine	UA	PBS	468	2340 (± 85.5)	2558 Fig. S3

Table 2 shows a comparison of the features of the proposed sensor with others proposed in the literature for the simultaneous detection of ascorbic and uric acid. Table 2 shows that, in many cases, the sensors have a high sensitivity only towards one of the two acids. The sensor here obtained shows a high sensitivity both for uric and ascorbic acid in a good linear range and with a low LOD.

Table 2 Comparison of sensor's features with other sensor for simultaneous detection of AA and UA
MTA: methenamine, Glu: Glucose, Glut: Glutathione, Cys: L-Cysteine, FA: Folic Acid, LDA: Levodopa, DA: Dopamine,CA: citric Acid, Gly: Glycine, GA: Glutamic Acid, FG: Fibrinogen, FBS: Fetal Bovine Serum, TA: Tartaric Acid, Tyr: Tyrosine, PImox: overoxidized-polyimidazole, GCE: Glassy Carbon Electrode, GS: Graphene Sheets, PTCA: 3,4,9,10-perylenetetracarboxylic acid, AzA: Azure-A, MWCTs: Multi Walled Carbon Nanotubes, S-CE: sonogel–carbon electrodes, NPG: Nanoporous Gold, CFP: carbon Fiber Paper, rGO: reduced graphene oxide, Gr:Graphene, ITO: Indium Tin Oxide, Pr: poly(3,4-ethylenedioxythiophene), GO: Graphene oxide, N.S.: not studied

Active Material	***Linear Range μmol dm^{-3}***	***Sensitivity μA μmol^{-1}dm^3 cm^{-2}***	***LOD μmol dm^{-3}***	***Interference***	***Real Sample***	***Ref***
AuNPs/PImox/GCE	*AA:* 210-1010 *UA:* 6-486	*AA:* 0.126 *UA:* 0.256	*AA*: 2 *UA:* 0.5	Na^+, K^+, Cl^-, Ca^{2+}, Mg^{2+}, SO_4^{2-}, MTA, EDTA, Glu, Cys, FA, LDA, Glut	Urine, serum, Vitamin C Tablet	[76]
GS–PTCA	*AA:* 20-420 *UA:* 4-544	*AA:* 0.204 *UA:* 0.79	*AA*: 5.6 *UA:* 0.92	DA, Tyr	N.S.	[77]
AzA/MWCNTs/AuNPs	*AA:* 300-10^4 *UA:* 0.5-50	*AA*: 0.04 *UA:* 20.03	*AA*: 16 *UA:* 0.01	Na^+, K^+, Ca^{2+} Mg^{2+}, CA, TA, Glu	Urine, Milk	[78]
S-CE/l-Cys	*AA:* 10-100 *UA:* 50-1000	*AA*: 0.684 *UA:* 0.241	*AA*: 50 *UA:* 10	N.S	Human Serum	[79]
NPG	*AA:* 320-3400 *UA:* 65-1500	*AA*: 0.116 *UA:* 0.245	*AA*: 63 *UA:* 9	FG	FBS	[80]
AuNPs@MoS2 nanosheets/GCE	*AA:* 20-300 *UA:* 20-400	*AA*: 0.48 *UA:* 0.46	*AA*: 3 *UA:* 5	Glu, Gly, GA	Human serum	[81]
Pt@NP-AuSn/CFP	*AA:* 200-1200 *UA:* 25-500	*AA*: 0.4 *UA:* 0.3	*AA*: 5.51 *UA:*0.67	K^+, Cl^-, Na^+, NH_4^+, Glu, Gly, CA	Urine	[82]
PdNPs/rGO/GCE	*AA:* 500-3500 *UA:* 15-42	*AA*: 0.08 *UA:* 0.481	*AA*: 100 *UA:* 16.67	Na^+, Cl^-, Mg^{2+}, SO_4^{2-}, Glu	Human serum	[83]
ZnO-rGO-GCE	*AA:* 1-5000 *UA:* N.S.	*AA*: 0.178 *UA:* N.S.	*AA*: 10 *UA:*N.S.	N.S.	Vitamin C Tablet	[35]
ZnO-Gr/ITO	*AA:* N.S. *UA:* 5-80	*AA*: N.S. *UA:* 0.3	*AA*: N.S. *UA:*0.01	N.S.	Urine	[84]
Pr-GO	*AA:* 500-1000 *UA:* 1-300	*AA*: 0.053 *UA:* 1.41	*AA*: N.S. *UA:* 0.19	N.S.	Urine	[36]
ITO-rGO-AuNPs	***AA:* 20-150** ***UA:* 10-500**	***AA*: 0.153** ***UA:* 0.31**	***AA*: 9.4** ***UA:* 10.9**	**DA, Na^+, Cl^-, NH_4^+, K^+, NO_3^-**	**Milk, Juice, Urine**	**This work**

4. CONCLUSIONS

rGO-AuNPs based electrodes were fabricated by co-electrodeposition on ITO substrate. Electrodes were tested for the detection of uric acid and ascorbic acid. Sensors were fully characterized by means of several techniques, which revealed the deposition of Au nanoparticles covering the r-GO sheets. The particular obtained morphology ensures a high surface area, as demonstrated by the the double layer capacitance evaluation. Electrodes were tested at different pH, showing better performance at pH 8 for both UA e AA. Calibration line was calculated at this pH, showing a linear relation in the range from 10 to 500 µmol dm^{-3} for UA with R^2 of 0.998 and a sensitivity of 0.31 µA cm^{-2} μM^{-1}. For AA the linear range was comprised between 20 µmol dm^{-3} and 150 µmol dm^{-3} (R^2 0.997) with a sensitivity of 0.118 µA μM^{-1}. The calculated values of LOD were 3.6 µmol dm^{-3} and 3.1 µmol dm^{-3}, respectively for UA e AA. The simultaneous detection of UA and AA was also studied. Good results were achieved with LOD of 2.26 and 5.63 µmol dm^{-3} respectively, without loss in sensitivity but in a lower linear range. The found limits are lower enough, compared with the main respective values in food and human fluids, to enable the application of the sensor in both health care and food industry. Sensors were also validated in real samples of milk, fruit juice and urine. The results appear good and comparable to values obtained by using standard technique. Besides, the sensors showed good selectivity toward different interfering species present in the matrix of milk, fruit juice and urine (dopamine, Na^+, NH_4^+, Cl^- and glucose). The stability, reproducibility and repeatability were also evaluated, showing that the sensors have very good features.